jet INTL JOURNAL OF ELECTRONICS AND TELECOMMUNICATIONS, 2011, VOL. 57, NO. 1, PP. 9–14
Manuscript received January 19, 2011; revised February 2011. DOI: 10.2478/v10177-011-0001-3

Radar Signatures of Complex Buried Objects in Ground Penetrating Radar

Berthold Panzner, Andreas Jöstingmeier, and Abbas Omar

***Abstract*—The evaluation of radar signatures of buried objects for three experimental ground penetrating radar setups will be addressed in this paper. The contribution will present corresponding results and experiences. The performance of the imaging capabilities of the designed radar system will be assessed by reconstruction of complex shaped test objects, which have been placed within the ground. The influence of system parameters of the ground penetrating radar have been varied systematically in order to analyze their effects on the image quality. Among the modified parameters are the step size in transverse plane, height of the antenna over ground, frequency range, frequency points, antennas and varying instrument settings. A signal processing technique based on synthetic aperture radar has been applied on the measured raw data. The focus radius around a specific target has been analyzed concerning the compromise between image quality and processing time. The experiments demonstrate that the designed ground penetrating radar systems are capable for detection of buried objects with high resolution.**

***Keywords*—Image reconstruction, inverse scattering, synthetic aperture radar, GPR, migration.**

I. Introduction

GROUND Penetrating Radar (GPR) is a technique for sensing visually obscured objects and has evolved a variety of applications for civil as well as military use. The field of applications spans over geological surveys, crack detection in runways and concrete, borehole radar, glacier ice thickness surveys to mine detection [1]. As a matter of fact, in all GPR scenarios the target is located in the lower half space, surrounded by an inhomogeneous permittivity distribution of the ground, whereas the antenna and radar system is located at a certain height above the air-soil interface without having a direct contact to it. Fig. 1 shows the laboratory GPR test facility which has been developed at the Chair for Microwave Engineering of the University Magdeburg. This paper is an extended version based on [2] and presents three different ground penetrating radar setups and stress the focus on practical experiences with these systems with respect to the detection of buried test objects. We will examine the influence of different settings and parameters on the radar performance. The performance of a GPR system is expressed in terms of image resolution and penetration depth. Hereby resolution is roughly speaking the ability to separate between different objects. In imaging radar applications, the term resolution is distinguished in range resolution, i.e. the resolution in vertical direction and cross range resolution, i.e. the lateral resolution perpendicular to the direction of propagation. Range resolution is the separation in the direction of propagation and is related to the bandwidth of the used radar. In contrast, cross range resolution (spatial resolution) is related to the area onto the ground surface, which is illuminated by the antenna. Usually the buried target objects are small, so that the natural resolution for common GPR setups is not sufficient. In order to increase the spatial resolution additional post-processing techniques such as synthetic aperture radar (SAR) have to be applied on the unfocused raw data. A SAR focusing technique that takes into account the refraction of the antenna beam into the ground will be presented. The performance of the proposed SAR technique will be assessed by image reconstruction of known test objects, that have been placed in the test site. The reconstruction of the shape of the objects is a measure of the quality of the used imaging radar setup.

The authors are with the Chair of Microwave and Communication Engineering, Otto-von-Guericke University of Magdeburg, P.O. Box 4120, 39016 Magdeburg, Germany (e-mails: panzner@ieee.org, andreas.joestingmeier@ovgu.de, a.omar@ieee.org).

II. Measurement Procedure

The laboratory GPR test facility consists of a sand-filled box, an antenna positioning system and a vector network analyzer (VNA). This so-called instrumentation setup is shown in Fig. 1. A portable GPR setup with handheld instruments (Rohde & Schwarz FSH-6 and Anritsu MS2028B) has also been installed on a movable platform for in-situ measurement (Fig. 2 and Fig. 3). In order to perform a radar scan of a buried object a so-called monostatic instrumentation setup is used, i.e. a VNA measures the reflection coefficient of a single antenna.

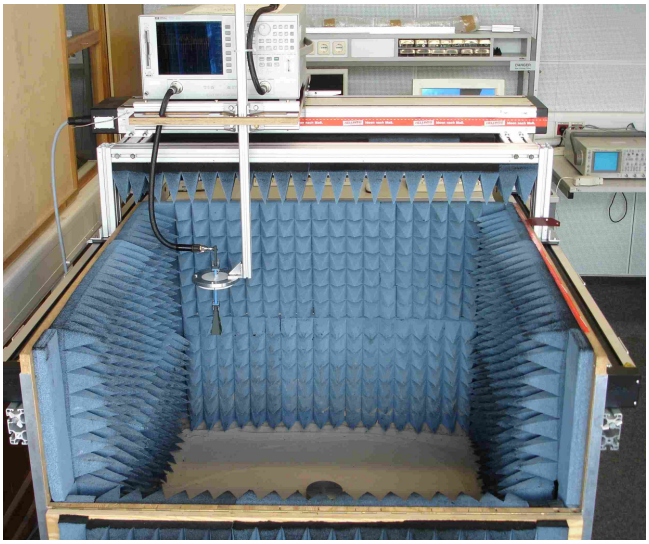

Fig. 1. Laboratory GPR Setup with stationary equipment.

Fig. 2. Mobile GPR Setup with R&S FSH-6 in outdoor measurement.

Thus only a one port measurement of S_{11} is performed. The antenna is moved above the ground to scan a certain area of the ground surface. At each antenna position a complete sweep over a specified bandwidth in stepped frequency continuous wave (SFCW) mode is performed. A view graph, that illustrates the measurement procedure based on a system model is shown in Fig. 4. The instrumentation setup makes use of a reflectometer, which measures the reflected signal at a single feeding port. Among the parameters, which can be modified in the setup are the start and stop frequency, the discrete number of frequency points, the IF bandwidth (RBW) of the VNA and the step width of the moving antenna of the antenna positioning system. For the three tested setups also various antennas in different heights have been used according to the frequency range of the corresponding VNA.

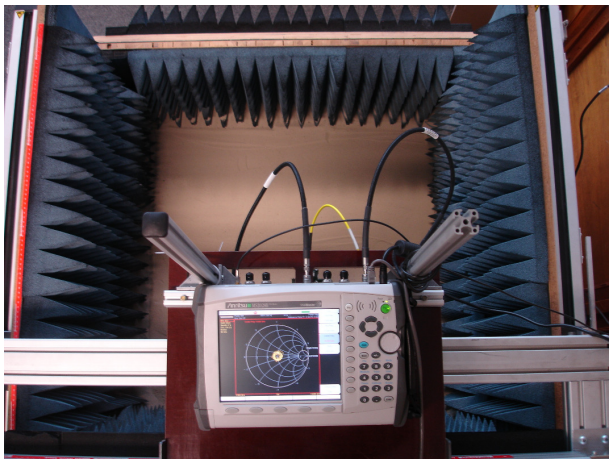

Fig. 3. Top view of GPR facility with portable Anritsu MS2028B.

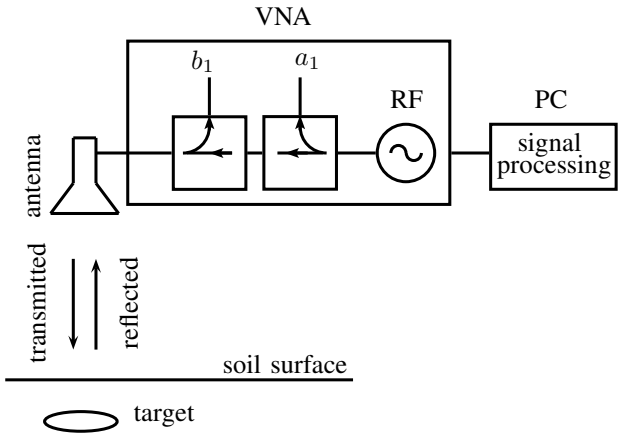

Fig. 4. GPR system model for a monostatic instrumentation setup.

III. Experimental Setup

For the detection of non-metallic buried objects three measurement setups have been used in total. In this section we will discuss the influence of the instrument settings and parameters on the measurement result. A comparison of all three instruments used in our GPR experiments is collocated in Table I. The stationary setup with the HP8722D allows a wide range of operating frequencies, since this instrument spans a frequency range up to 40 GHz. Experiments with the HP8722D in the Ka-band (26-40 GHz) have revealed high range resolution, capable to detect anti-personnel-landmines [3]. The measurement bandwidth in the frequency domain determines the resolution in range domain. In order to increase the detection probability especially for geometrical small objects a bandwidth of several GHz is necessary. The spectral density (number of frequency points per bandwidth) of the measurements limits the depth of the sampled data. Assuming a certain bandwidth, the spectral density is proportional to the number of frequency points. In practice most of the buried objects are closely located to the soil surface and it is not necessary to measure a dense spectrum. Typically the number of frequency points has been set to 401 in the tested GPR scenarios. For the HP8722D setup the measured data is transferred via GPIB to a PC. The processing of the raw data will be discussed in Section IV. The second setup utilizes a handheld spectrum analyzer (FSH-6), which is extended with a VSWR bridge. The build-in directional coupler of the optional VSWR bridge (FSH-Z3) allows to use the spectrum analyzer

TABLE I
Instruments Setups for GPR

instr.	HP8722D	R&S FSH6	MS2028B
manufacturer	Agilent	Rohde & Schwarz	Anritsu
instr. type	Network Analyzer	Spectrum Analyzer	Network Analyzer
freq.	50 MHz - 40 GHz	100 kHz - 6 GHz	5 kHz - 20 GHz
IF BW	10 Hz - 6 kHz	100 Hz - 1 MHz	10 Hz - 100 kHz
freq. points	selectable max 1601	fixed 301	arbitrary max 4001
data transfer	GPIB	RS232 serial	Ethernet (TCP/IP)
memory	floppy	internal	USB
connector	test port cable	N	K
weight	heavy (25kg)	portable (4 kg)	portable (5kg)
power	power line	battery (NiMH)	battery (Li-Ion)

in conjunction with its integrated tracking generator as one-port network analyzer (reflectometer). However in network analyzer mode the frequency settings of the instrument are limited, e.g. the number of frequency points is fixed. The portable GPR setup with the FSH-6 has been used for outdoor in-situ measurements. The upper frequency limit of the FSH-6 of 6 GHz is sufficient for most GPR applications. The transmission of the measured data to a laptop is done via optical serial connection. The third GPR setup is composed of the very advanced network analyzer Anritsu MS2028B. This true 2-port network analyzer is state of the art for handheld and battery powered instruments. The MS2028B covers a frequency range of 5 kHz to 20 GHz and a flexible frequency setting for IF bandwidth (RBW) and number of frequency points. An interesting feature is the build-in GPS receiver, which not only tracks the local position of the instrument but also serves as a precision reference oscillator. The measured data is transferred via Ethernet. The remote commands are based on the SCPI protocol and can be exchanged either over Ethernet or a USB connection. The MS2028B is a verstile and suitable setup for the GPR experiments performed with the test facility shown in Fig. 3. Due to flexible network connection the computer for signal processing purposes can be located at another position. A variety of antenna designs and concepts have been applied to the presented GPR setups. The antenna is a vital part within a GPR environment and has to be chosen according to the specific task. In [4] an overview of common GPR antennas is given. Among the typical used antennas are bow-tie antennas [5], modified impulse radiating antennas [6] and double-ridged horn antennas. A double-ridged horn antenna [7] for 1-6 GHz has been designed especially for use with the FSH-6. Another concept of a GPR antenna is a lens antenna [8]. A dielectric lens is used to focus the beam that illuminates the area on the ground surface. By focusing the waves onto a small spot the spatial resolution is increased. Thus the inherent focusing nature of a dielectric lens has a similar effect on the image resolution as focusing by means of synthetic aperture radar. A comparison of a dielectric lens and SAR technique for Ka-band (26-40 GHz) is presented in [9].

IV. Signal Processing

The necessary processing steps to receive a radar image from a measurement are listed schematically in Fig. 5. The measured radar raw data can be considered as a three-dimensional data array that is composed of the frequency domain data of each measurement point. The radar is moved above the soil surface in order to scan in the x-axis and the y-axis and perform a complete frequency sweep at each position. Thus each element of the three-dimensional matrix (*number of x-positions* $\times$ *number of y-positions* $\times$ *number of frequency points for* S_{11}) contains the measurement result of the reflection coefficient. The transferred data of the complex S_{11} is multiplied with a Gaussian pulse of the same bandwidth as the measured bandpass signal (see Fig. 6). This is done in order to remove any periodicity that results from the discrete version of the Fourier transform. However, if the bandpass

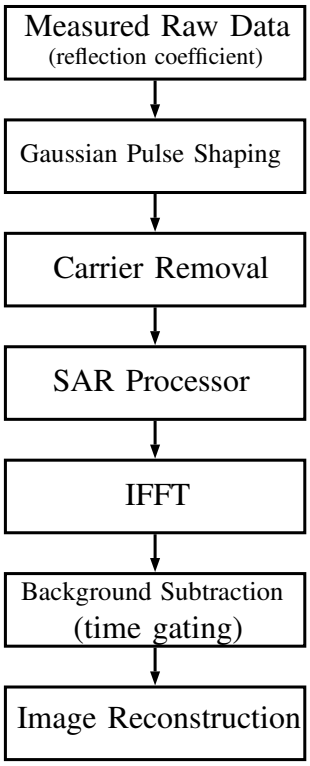

Fig. 5. Signal-processing methodology.

signal would be windowed by a rectangular window it results in a $\frac{\sin(x)}{x}$ behavior after Fourier transform, which results in multiple ghost replicas of the target. After the bandpass signal is shifted to an equivalent low-pass signal it is inverse Fourier transformed. The data set of measured frequency samples is transformed into a data set of corresponding time samples at each of the measurement positions. By determination of the propagation velocity of the wave in air and in soil the time samples can be translated into a distance. To further increase

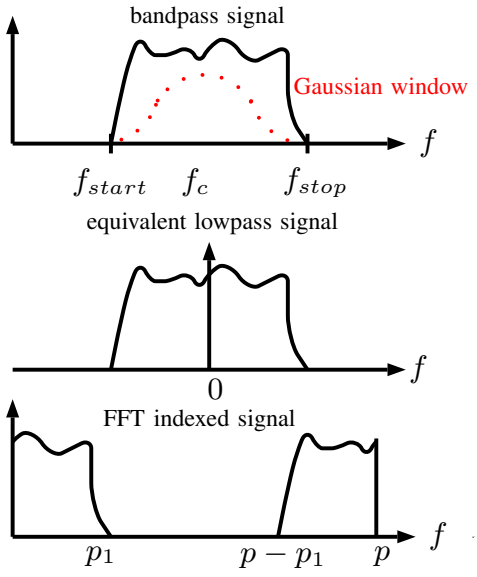

Fig. 6. Signal-processing of radar raw data.

the the spatial resolution of the unfocused microwave images, additional signal processing techniques like synthetic aperture radar (SAR) are necessary. SAR is a post-processing technique, that combines all received reflections of a target from different illuminating positions [10]. The phase difference of the individual signals are compensated according to their electrical path length. The superposition of the consecutively measured data results in focused beam of higher spatial resolution. The problem of forming subsurface radar images by means of synthetic radar aperture regarding the exact path of propagation is addressed in [11]. Due to the different permittivities at the media boundary of the air-soil interface, the electromagnetic wave is refracted into the soil. The correct path length is thus dependent on the relative permittivity of the soil.

V. Synthetic Aperture Radar Processing

Synthetic aperture radar is a post processing technique that combines all received reflections of a specific target from different illuminating positions (see Fig. 7). This procedure synthesizes a virtual antenna array that has a larger (synthetic) aperture than the real aperture of the single antenna element and consequently has improved lateral (cross range) resolution. This can be achieved by multiplying the measured data set $S(x, y, f)$ for each individual measurement position (x, y) by a phase correction term $h(x - x_F, y - y_F)$. The argument of the phase term represents the path length from the antenna position (x, y) to the focal point (x_F, y_F) within the ground. The SAR focused data set is denoted by $U(x_F, y_F, f)$. For a single target inside the soil this equates to:

$$U(x_F, y_F, f) = \iint_{xy} S(x, y, f) e^{j2kh(x-x_F, y-y_F)} dxdy \quad (1)$$

where $S(x, y, f)$ is the measured (unfocussed) raw data and the exponential term in eq.(1) corresponds to the phase correction. A forward propagating electromagnetic wave in the z-direction is expressed by the exponential e^{-jkz}. To compensate a phase offset due to different path lengths, one has to correct the signal with a phase term of opposite sign $e^{+jkz_{corr}}$. The phase correction term has to be evaluated for the path in air $e^{j2k_0 l_{air}}$ and the path inside the soil $e^{j2k_{soil} l_{soil}}$ separately, where l_{air} denotes the path length in air and l_{soil}

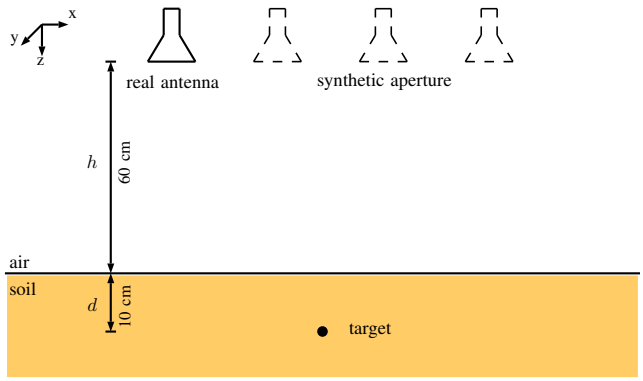

Fig. 7. GPR system model for Synthetic Aperture Radar.

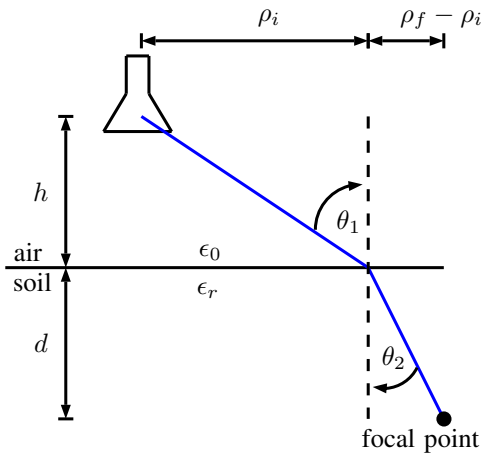

Fig. 8. Geometry of propagation path for delay compensation.

in soil, respectively. The factor 2 in the argument of the complex exponential results from the round trip delay. Since the focusing procedure has to be done for every focal point in the same transversal plane (a certain depth d), the total sequence for a complete C-scan (z-cutting plane) results in 4 hierarchical loops for discrete data sets, namely over the x- and the y-axis of the measured data and again over the the x- and the y-axis of the focusing matrix. The phase compensation of the corresponding path length from each individual source point to a single focal point within the ground can be derived from the geometric relations in Fig. 8. The point of penetration into the ground is determined by finding the root of Snell's law [12]:

$$\begin{aligned} \frac{\sin\theta_2}{\sin\theta_1} &= \frac{1}{\sqrt{\epsilon_r}} \\ \frac{\frac{\rho_f-\rho_i}{\sqrt{d^2+(\rho_f-\rho_i)^2}}}{\frac{\rho_i}{\sqrt{h^2+\rho_i^2}}} &= \frac{1}{\sqrt{\epsilon_r}} \\ \frac{(\rho_f-\rho_i)\, h \sqrt{1+\left(\frac{\rho_i}{h}\right)^2}}{\rho_i\, d \sqrt{1+\left(\frac{\rho_f-\rho_i}{d}\right)^2}} &= \frac{1}{\sqrt{\epsilon_r}} \end{aligned} \quad (2)$$

This equation has to be solved for ρ_i, which is actually a fourth order equation, with the parameters given in Fig. 8. For the SAR processing a specific target depth has to be chosen, i.e. the focusing is performed in a certain plane at a constant z-coordinate. Since the SAR processing will account for additional phase offsets compared to the propagation delay of the path perpendicular to the antenna over ground the corresponding phase correction, that compensates the different round-trip time delays equates as follows:

$$\Delta\phi_{(n)(m)} = e^{+j2k_0\left(\sqrt{h^2+\rho_{0(n)(m)}^2}-h+\sqrt{\epsilon_r}\left(\sqrt{d^2+\rho_{s(n)(m)}^2}-d\right)\right)} \quad (3)$$

with

$$\begin{aligned} \rho_{s(n)(m)} &= \sqrt{\left|x_{(n)} - x_{i_{(n)(m)}}\right|^2 + \left|y_{(n)} - y_{i_{(n)(m)}}\right|^2} \\ \rho_{0(n)(m)} &= \sqrt{\left|x_{i_{(n)(m)}} - x_{(m)}\right|^2 + \left|y_{i_{(n)(m)}} - y_{(m)}\right|^2} \end{aligned} \quad (4)$$

The index m represents the antenna positions in the plane of the antenna movement, whereas the index n represents the focal points in a specific z-plane. Details on the root finding of eq. 2 and the implementation of linearized goal function have been published in [11]. The time domain representation of the focused data that corresponds to the permittivity distribution inside the lower half-space is obtained by inverse Fourier transformation.

$$U(x_F, y_F, t) = \int_{-\infty}^{+\infty} U(x_F, y_F, f) e^{j2\pi f t} df \qquad (5)$$

If the permittivity of the surrounding medium is known the two way delay time of a scatterer can be translated into corresponding depths.

VI. Measurement Results

In order to evaluate the performance of the GPR setup and the proposed synthetic aperture radar focusing algorithm different test scenarios have been prepared. Fig. 9 shows a polystyrene test object, which has been buried at a depth of 7 cm. The unfocussed C-scan of the target is shown in Fig. 10. A C-Scan illustrates a two dimensional top view of the buried object in a certain depth. The radar signature of the same object after SAR processing is shown is Fig. 11. Note that both figures have been derived from the same radar raw data. The reconstruction of the non-metallic test-object after the SAR processor resembles the real object in an accurate manner. The presented radar image has been sampled with a step width of 1 cm in each direction (x-axis, y-axis). The reconstructed image is slightly blurred at the edges and shows the typical effect of a finite resolution. Nevertheless the SAR microwave image illustrates the shape and appearance of the real object with high accuracy. Other test objects have also been proven successfully with the presented GPR setups. The results are depicted in Fig. 12 for letter "E" object and in Fig. 13 for a zigzag object.

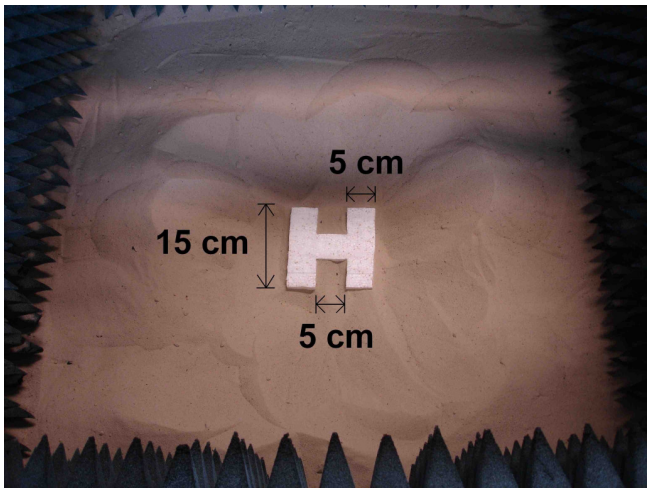

Fig. 9. Polystyrene test object (laid open for photography).

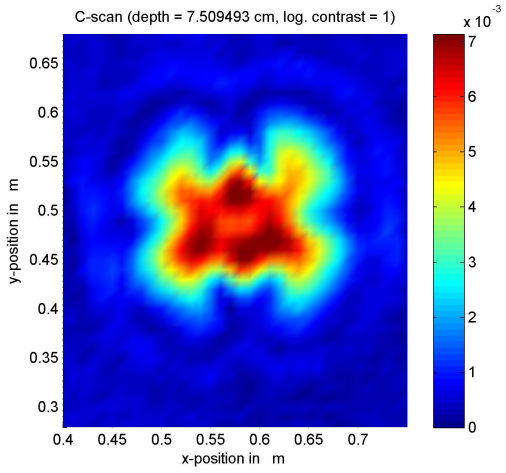

Fig. 10. Unfocussed raw radarscan of H-shaped object.

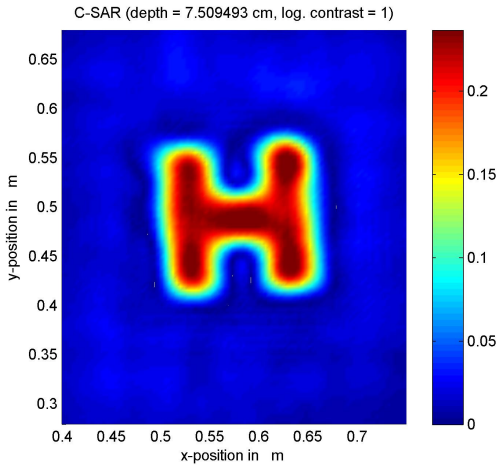

Fig. 11. SAR focussed radarscan of H-shaped object with 10cm focal radius.

VII. Conclusion

Experiences and recent results with three GPR setups for detection and reconstruction of visually obscured objects have

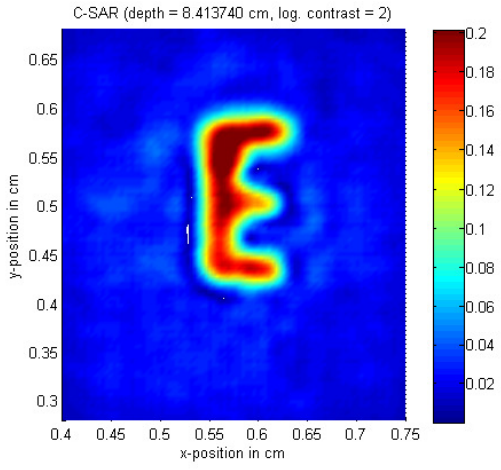

Fig. 12. Radarscan of E-shaped object.

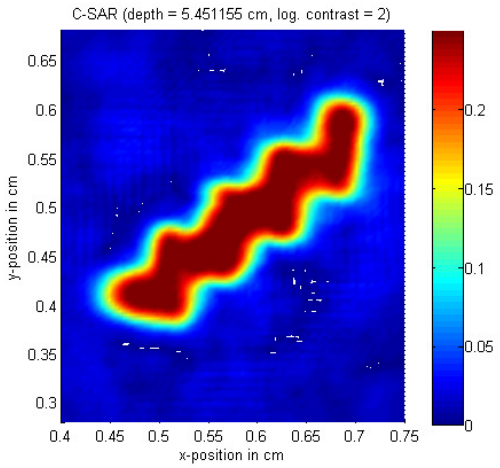

Fig. 13. Radarscan of complex zigzag object.

been presented in this work. An overview of the flexible setups, instrument settings and configuration for laboratory as well as portable GPR setups have been given. Various non-metallic objects have been placed inside the ground to evaluate the capability, to detect and identify the buried objects. By means of a synthetic aperture radar technique the image resolution of the measured raw data has been increased significantly. By using a focusing technique different non-metallic objects have been reconstructed with high spatial resolution. The capability to reconstruct the targets under various conditions has been demonstrated by measurements.

REFERENCES

[1] L. Capineri, S. Ivashov, and T. Bechtel, "Comparison of GPR Sensor Types for Landmine Detection and Classification," in *12th International Conference on Ground Penetrating Radar*, Birmingham, UK, June 16-19 2008.

[2] B. Panzner, A. Jöstingmeier, and A. S. Omar, "Radar Signatures of Complex Buried Objects in Ground Penetrating Radar," in *11th International Radar Symposium*, Vilnius, Lithuania, June 16-18 2010.

[3] ——, "Ka-Band Ultra-Wide-Band GPR for Landmine Detection," in *12th International Conference on Ground Penetrating Radar*, Birmingham, UK, June 16-19 2008.

[4] A. Yarovoy and et al., "Development of Antennas for Subsurface Radars within ACE," *IEEE Electron Device Lett.*, 2007.

[5] A. R. Bretones, "GA Design of a Thin-Wire Bow-Tie Antenna for GPR Applications," *IEEE Transactions on Geoscience and Remote Sensing*, vol. 44, no. 4, pp. 1004–1010, 2006.

[6] A. Teggatz, A. Jöstingmeier, and A. S. Omar, "A Forward Impulse Radiating Antenna for Subsurface Radars," *German Microwave Conference*, vol. Ulm, April 5-7 2005.

[7] B. Panzner, A. Jöstingmeier, and A. S. Omar, "A Compact Double-Ridged Horn Antenna for Ground Penetrating Radar Applications," in *18th International Conference on Microwaves, Radar, and Wireless Communications*, Vilnius, Lithuania, June 14-16 2010.

[8] A. Teggatz, A. Jöstingmeier, and A. S. Omar, "Application of a Dielectric Lens for Focusing of a GPR," *International Symposium on Antennas and Propagation*, vol. Honolulu, Haiwaii, June 10-15 2007.

[9] B. Panzner, A. Jöstingmeier, and A. S. Omar, "Ka-Band Dielectric Lens Antenna for Resolution Enhancement of a GPR," in *8th International Symposium on Antennas, Propagation and EM Theory*, Kunming, China, Nov 2-5 2008.

[10] V. Yakubov, D. Suhanov, and V. Kutov, "New Fast SAR Method for 3-D Subsurface Radiotomography," in *10th International Conference on Ground Penetrating Radar*, Deft, The Nederlands, June 21-24 2004.

[11] B. Panzner, A. Jöstingmeier, and A. S. Omar, "Evaluation of SAR Focusing Methods for Ground Penetrating Radar," in *8th European Conference on Synthetic Aperture Radar*, Aachen, Germany, June 7-10 2010.

[12] L. Zhou and Y. Su, "A GPR Imaging Algorithm with Artifacts Suppression," in *13-th International Conference on Ground Penetrating Radar*, Lecce, Italy, June 22-25 2010, pp. 331–336.